Influence of Lithium Ion Concentration on Electron Injection, Transport, and Recombination in Dye-Sensitized Solar Cells

James R. Jennings and Qing Wang*

Department of Materials Science and Engineering, Nanocore, National University of Singapore, Singapore 117574

Received: October 31, 2009; Revised Manuscript Received: November 24, 2009

Varying Li^+ concentration in the electrolyte of dye-sensitized solar cells equipped with compact TiO_2 blocking layers is found to alter the mean slopes of semilogarithmic open-circuit photovoltage−intensity and dark current−voltage plots. Almost identical values of ideality factor or transfer coefficient are required to fit data in the dark and under illumination for each Li^+ concentration. It is found that cell characteristics become progressively more "ideal" as Li^+ concentration is increased, with a transfer coefficient of ca.1 for 1 M Li^+ in the electrolyte. We find that trends in photovoltage−intensity data are well fitted using a model which assumes that electron transfer to acceptor species in the electrolyte occurs from both the conduction band of the TiO_2 and an exponential distribution of band gap surface states. Changes in the mean ideality factor and linearity of semilogarithmic photovoltage−intensity plots can be rationalized by considering the variation in overlap between occupied donor states (conduction band and surface states) with electron acceptor states in the electrolyte, as the conduction band edge is shifted positive by increasing Li^+ concentration. In accordance with previous studies, this positive shift in conduction band edge is also found to cause a dramatic increase in the photocurrent generation efficiency of the cells, especially in the long-wavelength region of the photocurrent action spectrum. It is argued that this improvement in photocurrent is predominantly due to an increase in wavelength-dependent electron injection efficiency, as opposed to an increase in electron collection efficiency.

Introduction

Dye-sensitized solar cells (DSCs)[1] have reached overall solar-to-electrical energy conversion efficiencies in excess of 11%.[2] A typical DSC consists of a mesoporous, nanocrystalline layer of TiO_2 supported on a transparent conductive oxide (TCO) substrate that provides an electrical contact to the TiO_2 as well as allowing light to enter into the cell. A layer of sensitizing dye (usually a ruthenium bipyridyl complex) is chemisorbed onto the surface of the TiO_2. This sensitized electrode acts as the light harvesting component of the solar cell and also facilitates transport of photogenerated carriers to the TCO. The sensitized TiO_2 electrode is attached to a platinum-coated cathode using a thin layer (25−50 μm) of a hot-melt polymer sealant. Permeating the pores of the TiO_2 and filling the interelectrode gap is a high ionic strength electrolyte containing a dissolved redox couple (usually the I_3^-/I^- couple).

The most highly efficient DSCs to date employ an electrolyte containing a variety of additives besides the basic I_3^-/I^- redox couple. One such additive is the Li ion, which is known to improve the photocurrent of DSCs while simultaneously reducing the open-circuit photovoltage. It is well-known that small cations such as Li^+ are potential determining for metal oxide electrodes and that specific adsorption of Li^+ results in a positive shift of the semiconductor energy levels. A number of studies have shown that this downward shift in the TiO_2 conduction band edge results in an increase in the efficiency of electron injection from the excited sensitizer.[3−6] This can be rationalized by considering the increase in the thermodynamic driving force for injection upon lowering the TiO_2 energy levels relative to the excited sensitizer energy levels, or in the Gerischer-type interpretation, a better energetic matching between sensitizer excited states and acceptor states in the TiO_2. Some studies indicate that this improvement in electron injection efficiency is wavelength dependent (implying significant injection from nonthermalized sensitizer molecules),[5,7] while others have found the electron injection efficiency is independent of wavelength while still varying with the conduction band edge position.[8]

The influence of Li^+ on charge recombination and collection in DSCs has not been studied as extensively as electron injection. Perhaps the most comprehensive study was carried out by Kopidakis et al. who found that intercalation of Li^+ into the nanocrystalline TiO_2 layer in DSCs increased charge recombination time constants while simultaneously increasing charge transport time constants, such that the overall charge collection efficiency remained practically unaffected.[9] We note however that the influence of trapping and detrapping of electrons in band gap states on these recombination and transport time constants was not explicitly considered.[10] For this reason we believe that the influence of Li^+ on the recombination characteristics of DSCs has not yet been unambiguously determined.

In this paper we present a detailed study of the effect of a systematic variation of Li^+ concentration on photocurrent generation efficiency, carrier recombination, and carrier collection in DSCs.

Experimental Methods

Fabrication of Dye-Sensitized Solar Cells. The dye-sensitized TiO_2 photoanodes used in this work were fabricated on fluorine-doped tin-oxide-coated glass (FTO, Pilkington TEC-8) cut into 1.5 cm × 2.5 cm pieces and cleaned by sequential sonication in 5% Decon 90 solution, distilled water, propan-2-

* To whom correspondence should be addressed. Corresponding author: qing.wang@nus.edu.sg.

10.1021/jp9104129
Published on Web 12/29/2009

ol, and absolute ethanol. Compact TiO_2 blocking layers were deposited on the FTO pieces by spray pyrolysis of a 0.2 M solution of titanium(IV) bis(acetoacetonato)diisopropanoxylate in ethanol. Spraying was carried out using a handheld aspirator with a spraying protocol of 2 sprays every 10 s for 4 min. Resulting TiO_2 thin films were determined to be ca. 100 nm thick by profilometry and scanning electron microscopy measurements. Electrodes were then soaked in a 40 mM solution of $TiCl_4$ in distilled water (prepared by dilution of a 2 M stock solution which was prepared at ca. 0 °C) for 30 min at 80 °C. After rinsing in distilled water and drying, a ca. 10 μm layer of nanocrystalline TiO_2 was deposited by successive screen printing using a commercially available TiO_2 paste (Dyesol 18NR-T). After screen printing, TiO_2 layers were gradually heated to 450 °C where they were held for 15 min before being heated to 500 °C for a further 15 min. Electrodes were subjected to a second identical treatment in $TiCl_4$ solution, rinsed, dried, and heated to ca. 450 °C in a hot air stream for 30 min. Once electrodes had cooled to ca. 100 °C, they were immersed into a 0.15 mM solution of *cis*-diisothiocyanato-(2,2′-bipyridyl-4,4′-dicarboxylic acid)-(2,2′-bipyridyl-4,4′-dinonyl)ruthenium(II) (Z907, Dyesol) in 1:1 acetonitrile:*tert*-butanol and left for 16 h before being removed and rinsed in acetonitrile.

Platinized counter electrodes were fabricated on identical pieces of FTO with small holes drilled into one corner. After cleaning, a thin layer of Pt was deposited onto the FTO by thermal decomposition of hexachloroplatinic acid.

Photoanodes and counter electrodes were sealed together in a sandwich configuration using a hot-melt polymer (Surlyn, DuPont). The interelectrode space was filled with an electrolyte by vacuum backfilling. Holes were sealed using a small piece of hot-melt polymer and a microscope coverslip. Electrolytes were all 1 M iodide and 0.1 M iodine in 3-methoxypropionitrile. Differing ratios of propylmethylimidazolium iodide (PMII) and lithium iodide were used in order to vary cation concentrations while maintaining nominally constant iodide concentration, ionic strength, and chemical constituents (type #1 electrolyte). A batch of cells employing 1 M PMII and varying amounts of lithium trifluoromethanesulfonimide (LiTFMSI) was also fabricated so that the concentration of the PMI^+ cation could remain constant while varying Li^+ concentration (type #2 electrolyte). Incident photon-to-collected-electron conversion efficiency spectra for the two batches of cells were found to be almost identical, and the influence of the Li^+ source on cell characteristics was not further studied. Data presented here were obtained for cells employing the type #1 electrolyte.

Characterization Techniques. Incident photon-to-collected-electron conversion efficiency (IPCE) spectra were measured with a spectral resolution of 5 nm using a 300 W xenon lamp and a grating monochromator equipped with order sorting filters (Newport/Oriel). The incident photon flux was determined using a calibrated silicon photodiode (Newport/Oriel). Photocurrents were measured using an autoranging current amplifier (Newport/Oriel). Control of the monochromator and recording of photocurrent spectra were performed using a PC running the TRACQ Basic software (Newport).

Dark current−voltage characteristics, photovoltage−intensity characteristics, and electrochemical impedance spectra were measured using an Autolab potentiostat/galvanostat and the Nova 1.5 software package. Illumination was provided by red (λ = 627 nm, 20 nm fwhm) and green (λ = 530 nm, 35 nm fwhm) high-power light emitting diodes (Luxeon). Illumination intensity was controlled using neutral density filters (Newport).

The thickness of nanocrystalline TiO_2 layers was determined by profilometry measurements made using an Alpha-Step IQ surface profiler. Optical transmission spectra of dye-sensitized TiO_2 layers were measured using a Shimadzu SolidSpec-3700 UV−vis−NIR spectrophotometer equipped with an integrating sphere. Absorption spectra of 100-fold dilute electrolyte solutions were measured using a Varian Cary 5000 UV−vis−NIR spectrophotometer.

Results and Discussion

Dependence of Incident Photon-to-Collected-Electron Conversion Efficiency Spectra on Li^+ Concentration. The incident photon-to-collected-electron conversion efficiency (IPCE) of a DSC can be defined as

$$\mathrm{IPCE}(\lambda) = \frac{j(\lambda)}{qI_0(\lambda)} = \eta_{\mathrm{lh}}(\lambda)\eta_{\mathrm{inj}}(\lambda)\eta_{\mathrm{col}}(\lambda) \qquad (1)$$

where $j(\lambda)$ is the photocurrent density, q is the elementary charge, $I_0(\lambda)$ is the incident photon flux, $\eta_{\mathrm{lh}}(\lambda)$ is the light harvesting efficiency of the sensitized TiO_2 layer (including losses due to the substrate transmission and electrolyte absorption), $\eta_{\mathrm{inj}}(\lambda)$ is the efficiency of electron injection from the excited sensitizer to the TiO_2, and $\eta_{\mathrm{col}}(\lambda)$ is the electron collection efficiency. Clearly the IPCE spectrum of a DSC contains information about light absorption, electron injection, and electron collection. Here we analyze IPCE spectra for DSCs containing different concentrations of Li^+ in the electrolyte in order to determine the origin of the enhancement in photocurrent brought about by addition of Li^+ to the electrolyte.

IPCE spectra were found to be strongly influenced by the presence of 10 mM−1 M Li^+ in the electrolyte, while spectra for 0 M and 1 mM Li^+ are almost identical (Figure 1a). The short-circuit photocurrent and open-circuit photovoltage were also found to increase and decrease respectively with increasing [Li^+] (Figure S1 and Table S1, Supporting Information).

Both peak IPCE and photocurrent onset wavelength increase with increasing [Li^+]. Spectra normalized to their respective peaks are practically identical for [Li^+] = 0−10 mM. Normalized spectra for [Li^+] = 0.1−1 M are the same to within experimental error for wavelengths below the peak, but a clear increase in IPCE can be observed at longer wavelengths (Figure 1b).

Normalization of the spectra effectively removes any wavelength-independent variations in the IPCE spectra between samples, such as sample-to-sample variation in substrate transmission or differences in any wavelength-independent component of the electron injection efficiency. The remaining differences between the spectra could in principle be due to differences in the wavelength dependence of any of the three partial quantum efficiencies making up the IPCE. Variations in $\eta_{\mathrm{lh}}(\lambda)$ caused by Li^+ have been ruled out by transmission measurements made on sensitized TiO_2 layers filled with electrolytes containing varying Li^+ concentrations (Figure S2, Supporting Information). These measurements also confirmed that the adsorbed sensitizer is capable of absorbing light up to wavelengths of 850 nm, in agreement with the IPCE data for the cell containing 1 M Li^+ in the electrolyte.

In principle η_{inj} could be a wavelength-dependent quantity if significant electron injection to the TiO_2 occurs before thermalization of the excited sensitizer.[7] Alternatively, the differences between spectra could be attributed to variations in $\eta_{\mathrm{col}}(\lambda)$ with the penetration depth of incident light due to a short electron diffusion length, which may vary with [Li^+].[6,8,11,12] In order to help distinguish between these two possible explana-

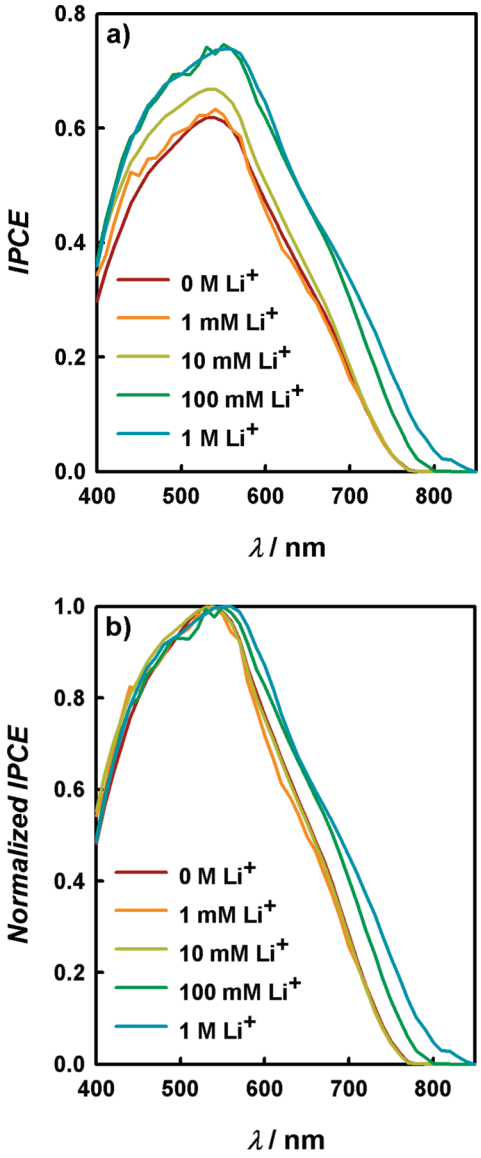

Figure 1. (a) IPCE spectra for DSCs containing 0 M (dark red), 1 mM (orange), 10 mM (dark yellow), 100 mM (dark green), and 1 M (dark cyan) Li^+ in the electrolyte. (b) IPCE spectra normalized to their respective peaks.

tions, IPCE spectra have been simulated using experimentally determined absorption coefficient spectra for the sensitized TiO_2 layers and a simple model based upon a continuity equation describing electron generation, diffusive transport, and recombination in the TiO_2 layer. This model was first applied to DSCs by Södergren et al. and has recently been used by several others to estimate electron diffusion lengths in DSCs by analysis of IPCE spectra.[6,8,11,12] According to this model the electron collection efficiency for substrate-side illumination is given by[12]

$$\eta_{col}(\lambda) = \frac{[-L\alpha(\lambda)\cosh(d/L) + \sinh(d/L) + L\alpha(\lambda)\exp(-\alpha(\lambda)d)]L\alpha(\lambda)}{[1 - \exp(-\alpha(\lambda)d][1 - L^2\alpha(\lambda)^2]\cosh(d/L)} \quad (2)$$

where L is the effective electron diffusion length, d is the TiO_2 layer thickness, and $\alpha(\lambda)$ is the effective absorption coefficient of the electrolyte-filled, sensitized TiO_2 layer. $\alpha(\lambda)$ for these cells was determined experimentally from transmission measurements of the electrolyte solutions and sensitized TiO_2 layers. It was assumed that the electrolyte occupied 50% of the volume

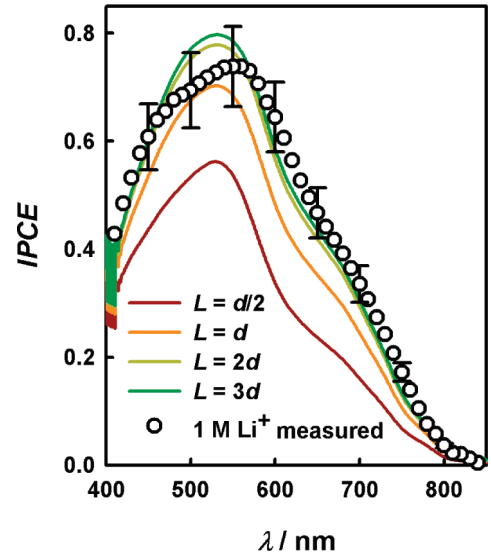

Figure 2. Simulated IPCE spectra, corrected to account for substrate transmission losses and absorption of light by the electrolyte, for $L = d/2$ (dark red), $L = d$ (orange), $L = 2d$ (dark yellow) and $L = 3d$ (dark green). Also shown is the experimentally determined IPCE spectrum for the DSC containing 1 M Li^+ in the electrolyte (open circles), including error estimates (for clarity, only included for every fifth data point) derived from the estimated uncertainty in the calibration of the reference photodiode.

of the TiO_2 layer, and light scattering effects were neglected. The light harvesting efficiency of the sensitized TiO_2 layer can be defined as

$$\eta_{lh}(\lambda) = T_{sub}(\lambda)\frac{\alpha_D(\lambda)}{\alpha(\lambda)}(1 - \exp(-\alpha(\lambda)d)) \quad (3)$$

where $T_{sub}(\lambda)$ is the transmission of the substrate and $\alpha_D(\lambda)$ is the absorption coefficient of the sensitized TiO_2 layer in the absence of the electrolyte.

Assuming a wavelength-independent η_{inj} equal to unity, IPCE spectra can be simulated using eqs 1−3 and experimentally determined data for $\alpha(\lambda)$, $\alpha_D(\lambda)$, and d. Figure 2 illustrates the effect of changing the electron diffusion length on the IPCE spectrum. Simulations include a correction for $T_{sub}(\lambda)$ which was estimated by transmission measurements of the substrates after deposition of the TiO_2 blocking layer. Also shown in Figure 2 is the experimental IPCE data for the 1 M Li^+ cell. Error estimates derived from the estimated uncertainty in the calibration of the reference photodiode have been included in the plot.

At wavelengths longer than 550 nm, the experimental data for the 1 M Li^+ cell is fitted very well assuming an electron diffusion length of greater than two times the TiO_2 layer thickness. Across all wavelengths the measured spectrum is consistent with $L \geq 2d$ to within the accuracy of our photon flux calibration. We therefore assume that both electron injection and electron collection in this cell are close to 100% efficient.

We find that IPCE spectra for cells with lower Li^+ concentration *cannot* be well fitted by assuming a wavelength-independent η_{inj} and varying the effective electron diffusion length. This is most clearly demonstrated by comparing simulated and experimental IPCE spectra, each normalized to their respective peaks to remove wavelength-independent variations between cells (Figure 3).

Clearly, the experimental spectra cannot be fitted by assuming that a change in electron diffusion length alone is responsible for the change in the shape of the IPCE spectra caused by varying Li^+ concentration. As mentioned previously, no change

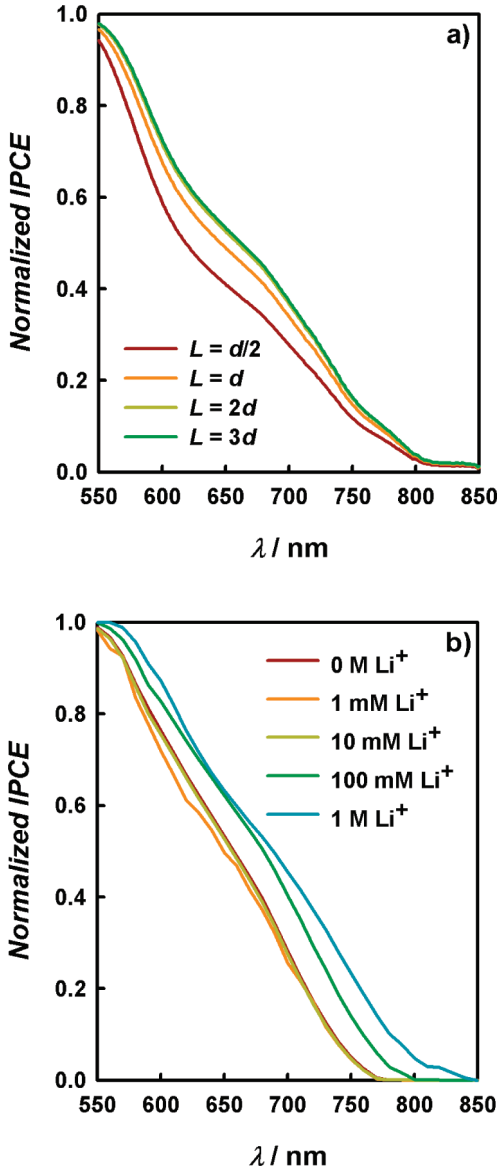

Figure 3. (a) Simulated IPCE spectra, normalized to their respective peaks, for $L = d/2$ (dark red), $L = d$ (orange), $L = 2d$ (dark yellow), and $L = 3d$ (dark green); (b) the same data shown in Figure 1b, reproduced for ease of comparison.

in the shape of transmission spectra of sensitized TiO_2 electrodes was observed upon varying Li^+ concentration. We therefore conclude that the increase in IPCE at long wavelengths, caused by increasing Li^+ concentration in the electrolyte, is predominantly due to an increase in the efficiency of electron injection. The fact that these wavelength-dependent differences between spectra are observed, which cannot solely be attributed to inefficient charge collection, implies that significant electron injection from nonthermalized sensitizer molecules must occur.

It should be noted here that the model used for simulating the IPCE spectra makes many, currently unverifiable, assumptions. These have recently been questioned and discussed in some detail by various authors.[6,8,12,13] The most important of these in the context of this work is that the recombination reaction is first order in TiO_2 electron concentration. It is expected that alternative recombination mechanisms will modify the shape of predicted IPCE spectra when electron transport is slower than recombination. However, as $\eta_{col}(\lambda)$ approaches unity, the shape of the IPCE spectrum must tend toward that predicted by $\eta_{lh}(\lambda)\eta_{inj}(\lambda)$, regardless of the detailed recombination mechanism. For this reason we believe our conclusions about the 1 M Li^+ cell remain valid. For the other cells we have shown, using an approximation which assumes recombination is first order in conduction band electron concentration, that changes in IPCE spectra are unlikely to be caused by variations in $\eta_{col}(\lambda)$. However, we believe that quantitative evaluation of charge collection losses is not possible at this stage, especially in light of the results and analysis presented in the following sections. Despite this, it seems unlikely that the marked shifts in IPCE onset wavelength with varying [Li^+] can be explained without invoking a significant wavelength dependence in the electron injection efficiency.

Influence of Li^+ Concentration on Electron Diffusion Length and TiO_2 Band Gap State Distributions. In order to confirm that electrons throughout the TiO_2 layer are collected with close to unit efficiency in these cells, a series of electrochemical impedance spectroscopy (EIS) experiments were performed with the aim of estimating the effective electron diffusion length for each cell. The experiments also provided a measure of the energetic distribution of band gap states in the TiO_2 for each of the cells, for comparison to results obtained from fitting photovoltage−intensity data to a recombination model which will be described in the next section.

EIS spectra were measured for all cells both in the dark as a function of bias voltage and as a function of incident photon flux ($\lambda = 625$ nm) with the cells biased such that the applied voltage was equal to the open-circuit voltage. In all cases a clear Warburg-like feature was observed at high frequencies in the Nyquist plot for spectra measured at intermediate voltages (Figure 4a), which can be attributed to electron transport in the TiO_2 layer.[14−16] For the case of an electron diffusion length which is comparable to or shorter than the TiO_2 layer thickness, the EIS spectra are expected to resemble a Gerischer impedance which was not observed for any of the DSCs studied here. At higher voltages the Warburg feature vanishes as the impedance due to electron transport becomes very small compared with other impedances in the cell (Figure 4b).

To obtain a quantitative estimate of electron diffusion length in these cells, EIS data were fitted using a transmission line model introduced by Bisquert et al. which describes the impedance of reaction and diffusion in a thin layer. The equivalent circuit used for data fitting is shown in Figure 4c. All capacitors were replaced with constant phase elements (CPEs) to improve the fits. Fitting results with an estimated uncertainty of greater than 20% or where the exponent of the distributed CPE did not fall in the range 0.9−1 were rejected as unreliable. Key model parameters which relate to processes occurring in the mixed TiO_2−electrolyte layer are the distributed chemical capacitance (c_μ), transport resistance (r_t), and charge transfer resistance (r_{ct}). The lowercase symbols used here represent distributed circuit elements which are related to the total capacitance and resistances of the TiO_2 layer by $C_\mu = c_\mu d$, $R_t = r_t d$, and $R_{ct} = r_{ct}/d$.

Fitting results for the cell with 1 M Li^+ in the electrolyte are plotted in Figure 5. The voltage scale for the dark EIS measurements has been corrected for *iR* drop across the series resistance of the cell.

As illustrated by Figure 5 the parameter values obtained for spectra measured in the dark and under illumination are similar at any given cell voltage. Values for the charge transfer resistance are found to be slightly lower (up to a factor of 2.3) under illumination compared with the dark values. This is likely to be due to an accumulation of photogenerated triiodide in the pores of the TiO_2 under illumination, reducing the effective

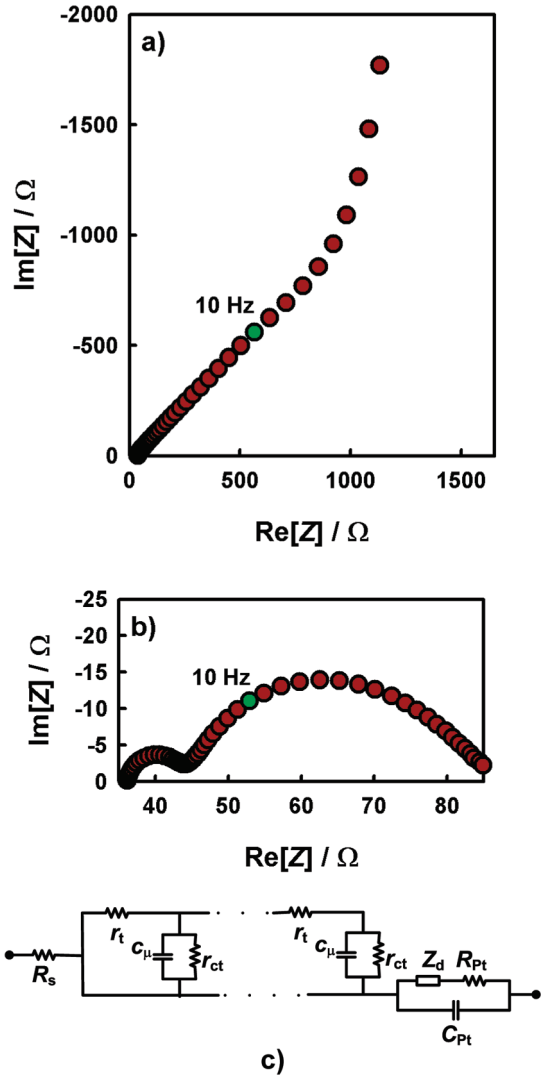

Figure 4. (a) High-frequency region of the Nyquist plot for cell containing 1 M Li^+ in the electrolyte, measured under illumination with $V_{OC} = 0.119$ V. The Warburg feature due to electron transport in the TiO_2 layer is clearly visible. (b) Complete Nyquist plot for cell containing 1 M Li^+ in the electrolyte. Measured under illumination with $V_{OC} = 0.440$ V. (c) Equivalent circuit used to fit EIS spectra.

electron lifetime. Other parameter values, including the transport resistance and chemical capacitance, measured in the dark and under illumination were also found agree to better than a factor of ca. 2 at any given voltage and Li^+ concentration. Based upon these results, we consider that changes in the rates of transport and interfacial transfer of electrons brought about by illumination are relatively unimportant in these cells.

The ratio of the electron diffusion length to the TiO_2 layer thickness can be estimated using the R_{ct} and R_t data by[17]

$$\frac{L}{d} = \sqrt{\frac{R_{ct}}{R_t}} \tag{4}$$

As expected from qualitative interpretation of EIS spectra, electron diffusion lengths in the range 2−5 times the TiO_2 layer thickness were found for all cells with the exception of the cell containing 1 M Li^+ in the electrolyte, where values of L fell in the range 10−15 times the layer thickness. In all cases charge collection is expected to be highly efficient, in agreement with the analysis of IPCE spectra for the 1 M Li^+ cell, and in support of the explanation that the observed enhancement in IPCE at

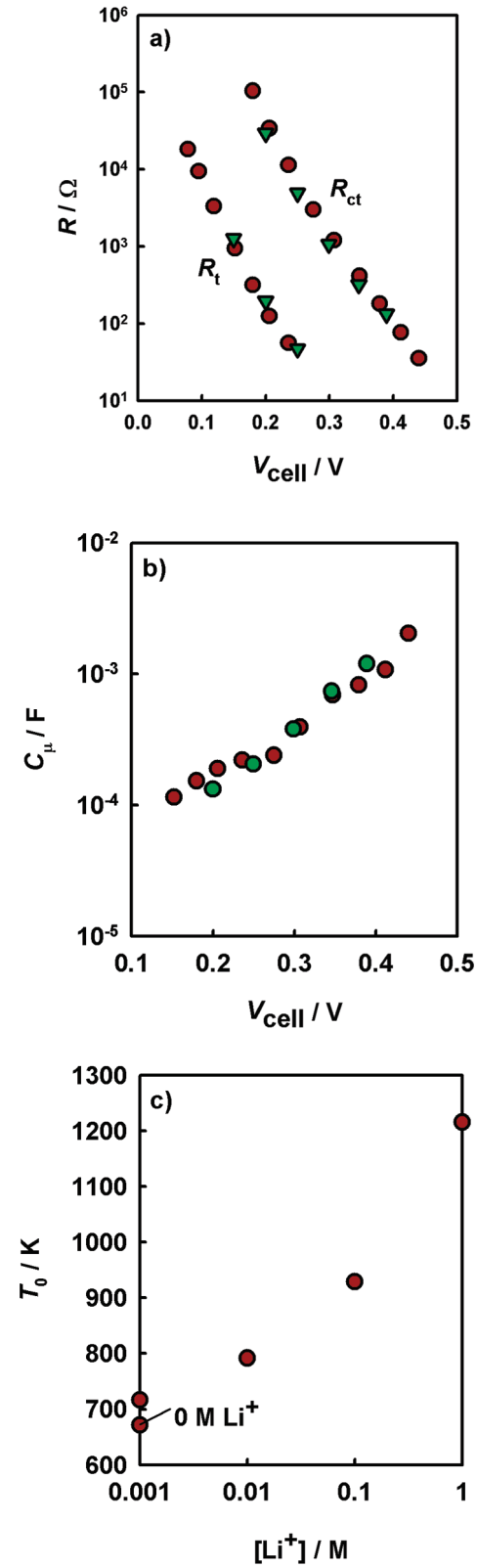

Figure 5. Plots of R_t, R_{ct} (a), and C_μ (b) versus cell voltage for the cell containing 1 M Li^+ in the electrolyte. Dark red and dark green symbols represent parameters measured in the dark and under illumination, respectively. The dependence of the band gap state characteristic temperature, T_0, on Li^+ concentration is also shown (c).

long wavelengths is due to improved electron injection as opposed to charge collection.

The capacitance, C_μ, contains contributions from the chemical capacitances of the conduction band, bulk band gap states, band

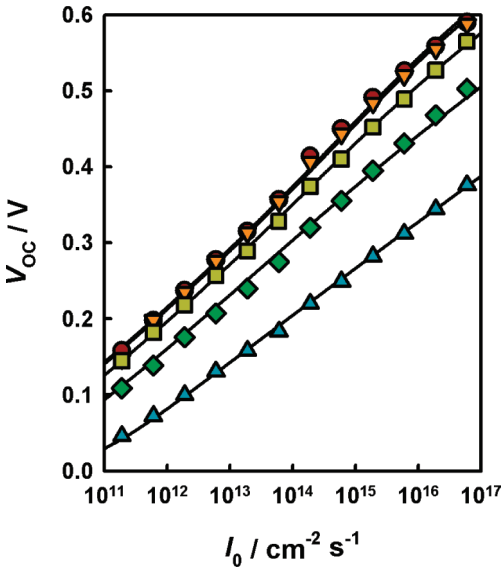

Figure 6. Plots of photovoltage versus incident photon flux ($\lambda = 530$ nm) for DSCs containing 0 M (dark red circles), 1 mM (orange triangles), 10 mM (dark yellow squares), 100 mM (dark green diamonds), and 1 M (dark cyan triangles) Li^+ in the electrolyte. Solid lines are fits to the model described in the text (fitting parameters can be found in Table 1).

gap surface states, and the Helmholtz capacitance. For the voltage range investigated here, contributions from the TiO_2 conduction band chemical capacitance and the Helmholtz capacitance are expected to be negligible so that C_μ provides a measure of the combined bulk- and surface-state chemical capacities. C_μ was found to vary approximately exponentially with cell voltage, and data have been fitted using the phenomenological expression

$$C_\mu(V_{cell}) = C_{\mu,0}\exp\left[\frac{qV_{cell}}{k_B T_0}\right] \quad (5)$$

where T_0 is a characteristic temperature, $C_{\mu,0}$ is a pre-exponential factor, and V_{cell} is either V_{OC} (for measurements performed under illumination) or the applied voltage (for dark measurements) after correction for iR drop across the series resistance of the cell. Values of T_0 for these cells fall in the range 671−1216 K and increase with increasing $[Li^+]$ (Figure 5c). The mean slopes of semilogarithmic $R_{ct}-V_{cell}$ and R_t-V_{cell} plots were also found to be influenced by $[Li^+]$ (Figure S3, Supporting Information). A weak trend of increasing $d\log_{10}(R)/dV_{cell}$ with increasing $[Li^+]$ was found for both R_{ct} and R_t.

Kopidakis et al. have also found that Li^+ intercalation alters the band gap state distribution and follows the same trend found here with increasing degrees of intercalation, although the range of characteristic temperatures (calculated from characteristic energies, m_c) reported by these authors, 707−4638 K, is much larger than we find here.[9] It is likely that the weaker variation in T_0 with increasing $[Li^+]$ is because significant Li^+ intercalation has not occurred (note that the bias voltage/photovoltage ranges studied here are relatively narrow compared with those studied by Kopidakis et al.) If it is assumed that both surface and bulk states have the same energetic distribution, then the characteristic temperature, T_0, can be identified with the characteristic temperature of the surface-state distribution, T_{ss}, which is a key parameter in the recombination models that will be discussed in the next section.

Influence of Li^+ on the Charge Recombination Mechanism. Figure 6 shows how varying Li^+ concentration influences the photovoltage−intensity characteristics ($\lambda = 530$ nm) of the cells studied.

TABLE 1: (a) Common Parameters Obtained from a Simultaneous Fit of All $V_{OC}-I_0$ Data (Figure 6) and (b) Variation in E_C with $[Li^+]$ Obtained from the Fitting Results[a]

Common Fitting Parameters	
λ/eV	0.721 ± 0.11
T_{ss}/K	710 ± 46
k_{cb}/cm^3 s^{-1}	$(9.12 \pm 19) \times 10^{-15}$
k_{ss}/cm^3 s^{-1}	$(1.26 \pm 0.076) \times 10^{-16}$
$[Li^+]$/M	E_C /eV
0	0.952 ± 0.031
0.001	0.946 ± 0.032
0.01	0.913 ± 0.035
0.1	0.845 ± 0.042
1	0.730 ± 0.054

[a] Fixed fitting parameters were $N_C = 10^{21}$ cm^{-3}, $N_{ss} = 10^{19}$ cm^{-3}, and $c_{ox} = 6 \times 10^{19}$ cm^{-3}.

As expected, V_{OC} values systematically decrease as $[Li^+]$ is increased, broadly consistent with a lowering of the conduction band energy of the TiO_2. However, an unexpected observation is that the mean slopes on the semilogarithmic plots also systematically vary with $[Li^+]$ as illustrated by Figure 7a.

Mean slopes on semilogarithmic dark current−voltage plots were found to be almost identical to those of semilogarithmic $V_{OC}-I_0$ plots ($\lambda = 625$ nm, measured during EIS experiments under illumination) over the same voltage ranges. Assuming $j_{dark} \propto \exp(qV_{cell}/mk_BT)$ and $I_0 \propto \exp(qV_{OC}/mk_BT)$, these mean slopes can be identified with the diode ideality factor, m, values of which are presented in Figure 7b. This finding implies that the recombination routes under illumination are essentially the same as those through which current flows in the dark when an external bias is applied to the cell, in agreement with the EIS experiments performed in the dark and under illumination. For this reason it seems justified to neglect electron transfer routes which are only possible under illumination (e.g., recombination with oxidized dye molecules) in the analysis of photovoltage−intensity characteristics for these cells.

The plots in Figure 6 for low Li^+ concentration are subtly curved, and the linearity of the plots increases with increasing Li^+ concentration. Both linear and nonlinear semilogarithmic photovoltage−intensity characteristics with mean slopes >59 mV/decade are frequently observed for DSCs. If recombination occurs solely via the conduction band of the TiO_2 and the reaction is first order in electron concentration, a linear plot with a slope of 59 mV/decade at 298 K is expected.[18] Clearly this explanation is only compatible with the data obtained for the cell with 1 M Li^+ in the electrolyte (highly linear plot, $dV_{OC}/d\log_{10}(I_0) = 59$ mV/decade for photovoltages above ca. 60 mV). It has been suggested that the nonideal photovoltage−intensity characteristics of DSCs can be explained by allowing for recombination via a distribution of band gap surface states, while also considering changes in the energetic matching between TiO_2 donor states and electron acceptor states in the electrolyte as the QFL varies, in accordance with Marcus−Gerischer electron transfer theory.[19,20] It has also been shown that recombination via the exposed FTO substrate can lead to curvature of semilogarithmic $V_{OC}-I_0$ plots; [21,22] however, we rule out this explanation in the present case since all DSCs used for this work were fabricated with compact TiO_2 blocking layers. Another suggestion is that the observed nonideality may be a

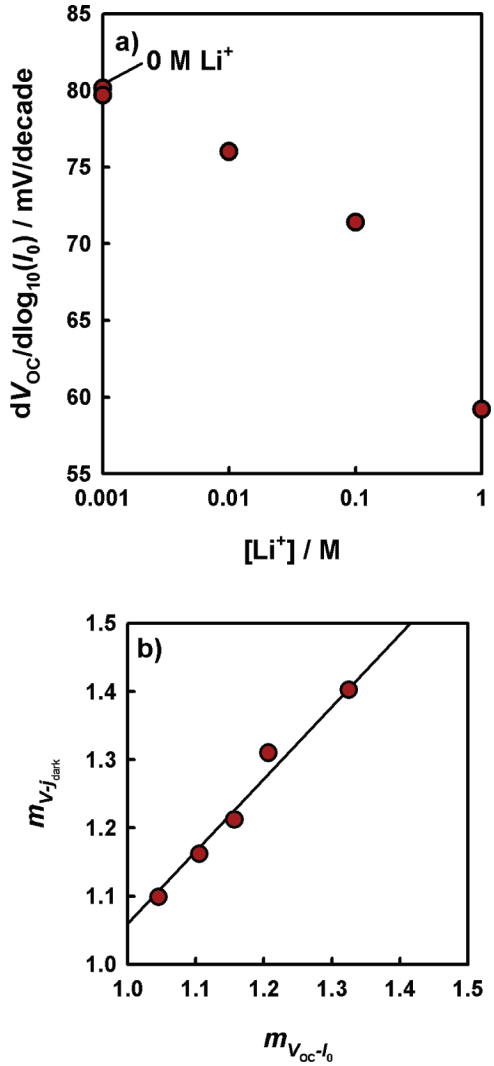

Figure 7. (a) Variation in the mean slopes of semilogarithmic $V_{OC}-I_0$ plots (Figure 6) with [Li^+]. (b) Comparison between ideality factors/transfer coefficients obtained from dark current−voltage characteristics ($m_{V-j\text{dark}}$, measured during dark EIS experiments) and $V_{OC}-I_0$ characteristics (m_{VOC-I0}, $\lambda = 625$ nm, measured during EIS experiments under illumination). Solid line is a linear fit forced through the origin, slope = 1.06.

result of nonideal electron statistics, rather than an indication of a recombination rate equation which is nonlinear in free electron concentration.[23] However, the exact physical basis for this last explanation is unclear at present, and so we do not further consider this possibility here.

In order to examine whether recombination via band gap surface states is a plausible explanation for the variation in photovoltage−intensity characteristics with [Li^+], data have been fitted to a model based upon that of Salvador et al. which describes the illumination intensity dependence of the photovoltage in DSCs.[20] This model is described in detail elsewhere,[19,20] and here we note only deviations of our approach to that of Salvador et al. and the expressions used in the data fitting.

Our model differs from that of Salvador et al. in several relatively trivial (but nevertheless important) ways. First, we do not consider electron transfer from deep monoenergetic surface states. We find that inclusion of this recombination route is not required to fit our data, and so the introduction of the additional fitting parameters and complexity into the model is not justifiable. We also allow the probability of electron transfer from the conduction band to depend upon the energetic matching between the conduction band edge and the electron acceptor distribution in the electrolyte, in accordance with Marcus−Gerischer theory and the model proposed by Bisquert et al. in ref 19. Salvador et al. do not explicitly include this in the model described in ref 20, but instead use the conduction band electron transfer rate constant as a fitting parameter. Finally, we define the pre-exponential factors used in the expressions for the electron transfer probabilities according to the expressions given in ref 19.

Under open-circuit conditions the total photogeneration rate of charge carriers, G, must equal the total recombination rate, U_{tot}.

$$G = \frac{I_0 \eta_{lh} \eta_{inj}}{d} = U_{tot} = U_{cb} + U_{ss} \tag{6}$$

where U_{cb} and U_{ss} are the rates of recombination via the conduction band and surface states, respectively. Assuming the rate of transfer of conduction band electrons to acceptor species in the electrolyte is first order in conduction band electron density, the rate of conduction band recombination is given by

$$U_{cb} = e_{ox}^{cb}(n_c - n_{eqm}) \tag{7}$$

where n_c and n_{eqm} are the conduction band electron densities under illumination and in the dark respectively. e_{ox}^{cb} is the probability of electron transfer from the conduction band to an electron acceptor in the electrolyte (e.g., I_3^- or I_2) and is given by

$$e_{ox}^{cb} = A_{cb} \exp\left[\frac{(E_C - E_{ox})^2}{4\lambda k_B T}\right] \tag{8}$$

where E_C is the energy of the conduction band edge, E_{ox} is the most probable energy level for the electron acceptor species (equal to λ if the energy origin is taken as the electrolyte redox level), λ is the reorganization energy, and A_{cb} is a pre-exponential factor given by

$$A_{cb} = \frac{2k_B T}{\sqrt{4\pi\lambda k_B T}} k_{cb} c_{ox} \tag{9}$$

where k_{cb} is the rate constant for electron transfer from the conduction band to acceptor species in the electrolyte and c_{ox} is the concentration of acceptor species in the electrolyte.

We assume that the conduction band electron density may be written in terms of V_{OC} and n_{eqm} as

$$n_c = n_{eqm} \exp\left(\frac{qV_{OC}}{k_B T}\right) \tag{10}$$

Substituting eq 10 into eq 7 yields the following expression for the conduction band recombination rate

$$U_{cb} = e_{ox}^{cb} n_{eqm} (\exp(qV_{OC}/k_B T) - 1) \tag{11}$$

If it is assumed that electron injection from the electrolyte to the TiO_2 may be neglected and that only band gap states in the TiO_2 below the electron quasi-Fermi level are filled (the 0 K approximation), the recombination rate from surface states is given by

$$U_{ss} = \int_{E_{F,redox}}^{{}_nE_F} N(E) e_{ox}^{ss}(E)\, dE \tag{12}$$

where $N(E)$ is the density of states function for band gap surface states in the TiO_2, $E_{F,redox}$ is the redox potential of the electrolyte, ${}_nE_F$ is the electron quasi-Fermi level, and e_{ox}^{ss} is the electron

transfer probability for surface states given by

$$e_{ox}^{ss} = A_{ss} \exp\left[\frac{(E - E_{ox})^2}{4\lambda k_B T}\right] \quad (13)$$

where A_{ss} is a pre-exponential factor given by

$$A_{ss} = \frac{2k_B T}{\sqrt{4\pi\lambda k_B T}} k_{ss} c_{ox} \quad (14)$$

where k_{ss} is the rate constant for electron transfer from surface states to acceptor species in the electrolyte.

Here we assume that the surface state distribution can be approximated by

$$N(E) = \frac{N_{ss}}{k_B T_{ss}} \exp\left[\frac{E - E_c}{k_B T_{ss}}\right] \quad (15)$$

where N_{ss} is the density of surface states at the conduction band edge and T_{ss} is the characteristic temperature of the distribution. For convenience, a tailing parameter can be defined as $\beta = T/T_{ss}$. Equation 15 can then be written as

$$N(E) = \frac{\beta N_{ss}}{k_B T} \exp\left[\beta \frac{E - E_c}{k_B T}\right] \quad (16)$$

The rate of recombination via this exponential distribution of surface states is obtained by substituting eqs 13 and 16 into eq 12 and integrating between $E = E_{F,redox}$ and $E = {}_nE_F$ (note that since $qV_{OC} = {}_nE_F - E_{F,redox}$ this is equivalent to integrating between 0 and qV_{OC}). Salvador et al. have shown that this expression can be transformed into the closed form (eq A2.3 in ref 20)

$$U_{ss} = C\left[\mathrm{erf}\left(\frac{a}{\sqrt{b}}\right) + \mathrm{erf}\left(\frac{qV_{OC} - a}{\sqrt{b}}\right)\right] \quad (17)$$

where $C = ((A_{ss}N_{ss}\beta\sqrt{\pi}\sqrt{b})/2k_BT)\exp(C_1)$, $C_1 = \beta E_{ox}/k_BT + \lambda\beta^2/k_BT - \beta E_C/k_BT$, $a = E_{ox} + 2\lambda\beta$ and $b = 4k_BT\lambda$ (note that there is a typographical error in the definition of the constant C in ref 20). If it is assumed that both conduction band electrons and electrons occupying surface states share a common quasi-Fermi level,[24] eqs 11 and 17 may be substituted into eq 6, resulting in an expression describing the relationship between I_0 and V_{OC}.

One major criticism of this model is that it has a large number of parameters, many of which cannot be readily determined experimentally. Nevertheless, there is a body of literature in support of this model,[17,19,20,25,26] and it is thus far the only quantitative model capable of explaining the curvature and nonideal slopes on semilogarithmic V_{OC} versus I_0 plots.

The approach to data fitting taken here minimizes the number of free fitting parameters and maximizes the overall number of degrees of freedom during the nonlinear regression, leading to a greater degree of statistical confidence in the fitted parameters. The parameters η_{lh}, η_{inj}, and d were experimentally determined by UV/vis, IPCE, and profilometry measurements ($\eta_{lh} = 0.98$, η_{inj} varied between 0.85 and 1 as [Li^+] varied between 0 to 1 M, and $d = 10$ μm). η_{inj} was estimated from the IPCE spectra assuming $\eta_{inj} = 1$ for [Li^+] = 1 M and $\eta_{col} = 1$ for all cells. Fits were also performed with $\eta_{inj} = 1$ for all cells, and results were found to be similar (parameters within ±25%); however, the approximate standard errors in the parameters increased and R^2 diminished slightly, so only the results obtained using the estimated values of η_{inj} are presented here. N_C was fixed to the theoretical value of ca. 10^{21} cm^{-3} for a semiconductor with parabolic band structure and an effective electron mass equal to the bare electron mass. We note that only the product of the parameters c_{ox}, k_{ss}, and N_{ss} appears in eq 12, and as such their individual values cannot be independently determined by fitting data using this model. Here c_{ox} is assumed to be equal to the concentration of I_2 added to the electrolyte (0.1 M, 6×10^{19} cm^{-3}), and we arbitrarily choose to fix the value of N_{ss} to 10^{19} cm^{-3} while allowing k_{ss} to vary as a fitting parameter.

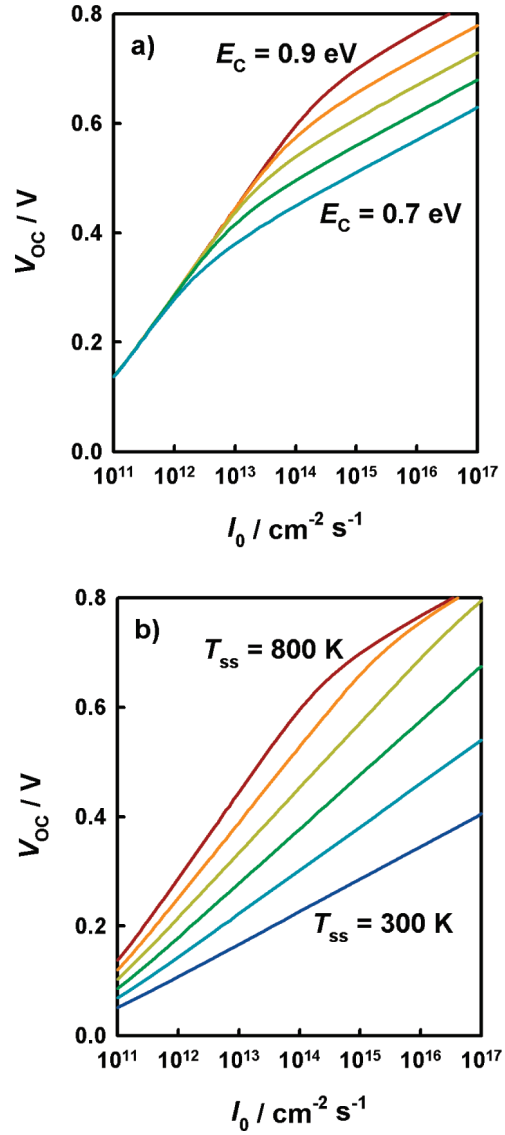

Figure 8. Simulated plots of photovoltage versus incident photon flux assuming global, energy-independent rate constants for electron transfer from the conduction band and surface states: (a) effect of varying E_C between 0.9 and 0.7 eV while keeping other parameters fixed; (b) effect of varying T_{ss} between 800 and 300 K while keeping other parameters fixed. Common model parameters: $N_C = 10^{21}$ cm^{-3}; $N_{ss} = 10^{19}$ cm^{-3}; $T_{ss} = 800$ K (plot a); $E_C = 0.9$ eV (plot b); $k_{cb,0} = 1$ s^{-1}; $k_{ss,0} = 10^{-6}$ s^{-1}.

All the V_{OC}–I_0 data obtained were fitted *simultaneously* using a method similar to that of Duggleby et al.[27] The parameters λ, T_{ss}, k_{cb}, and k_{ss} were common to all data sets, while individual values of E_C were allowed for each data set since this is the parameter expected to be most significantly influenced by introduction of Li^+ into the electrolyte. Based upon the EIS data presented in the previous section, the choice to fix T_{ss} to a constant value for all cells may be questioned. However, good fits could not be obtained by setting T_{ss} equal to the T_0 value derived from the EIS data for each cell. Allowing T_{ss} to vary

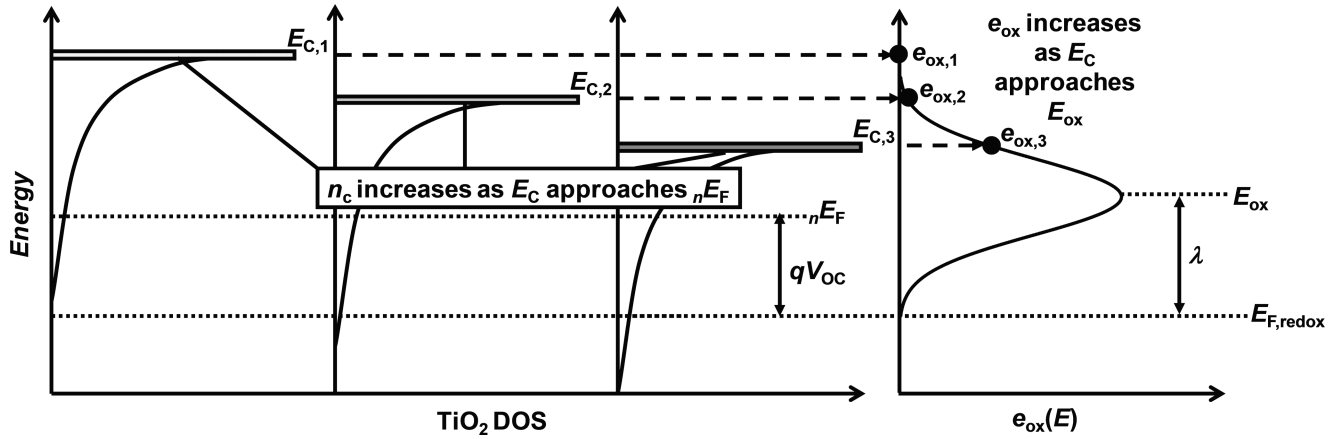

Figure 9. Diagram illustrating the effect of a downward shift in the TiO_2 conduction band energy ($E_{C,1}$ to $E_{C,3}$) at constant open-circuit voltage (V_{OC}). Both the conduction band electron density (n_c) and the Marcus−Gerischer transfer probability (e_{ox}) increase as the band edge shifts positive toward the electrolyte redox level ($E_{F,redox}$).

freely for each cell increased uncertainty in all fitting parameters while only marginally improving R^2. For this reason we believe that no additional physical insight is gained by allowing individual values of T_{ss} for each cell. The fitted data are plotted in Figure 6, and fitting parameters are listed in Table 1 along with their approximate standard errors.

Good fits to all data sets are obtained ($R^2 = 0.998$). The approximate standard errors in λ, T_{ss}, and k_{ss} are 15%, 7%, and 6% of the parameter values, respectively. For all fits the approximate standard errors in E_C are 3−7% of the parameter values. The approximate standard error in the value of k_{cb} is larger than the parameter value, and for this reason the value of k_{cb} should be considered somewhat arbitrary. We also find that, with appropriately linked changes in N_C and N_{ss}, the absolute values of k_{cb}, k_{ss}, and E_C are arbitrary. However, the *relative* values of these parameters (in particular the changes in E_C as $[Li^+]$ is varied, which is obtained with a high degree of statistical certainty) remain unaltered. We note that the value obtained for λ is physically reasonable and in agreement with previously reported values[17] and the value of T_{ss} falls in the range of those derived from the $C_\mu - V$ data (671−1216 K). As mentioned previously, fits were also performed with T_{ss} fixed to the values of T_0 derived from the EIS experiments, but good fits to all data could not obtained. This could be interpreted as evidence that the energetic distribution of surface states at the TiO_2−electrolyte interface is similar, but not identical to, the distribution of bulk states in the TiO_2.[19] Although the absolute values of the parameters obtained in this fitting may be questioned and require further independent corroboration, we believe this model has merit in that it simultaneously predicts both changes in the magnitude of V_{OC} and changes in the mean slopes of the plots by only varying a single parameter, E_C.

While clearly a model which assumes electron transfer only occurs through the conduction band is inadequate to explain the experimental data, it could be argued that use of the rather complex Marcus−Gerischer electron transfer model and the associated introduction of an extra fitting parameter, λ, is not justifiable. For this reason we have performed simulations using an approach taken by Cameron et al. and assumed a global, energy-independent rate constant for electron transfer via surface states.[22] We also assume that the value of the conduction band rate constant is independent of E_C. This is in contradiction with the Marcus−Gerischer theory which predicts the rate constant for transfer from the conduction band, while being constant with respect to the position of the electron quasi-Fermi level, should still vary with the position of the conduction band edge relative to the electrolyte redox level. We assume that the rate of recombination from the conduction band is given by

$$U_{cb} = k_{cb,0}(n_c - n_{eqm}) \tag{18}$$

and the rate of recombination from surface states by

$$U_{ss} = k_{ss,0} \int_{E_{F,redox}}^{{}_nE_F} N(E)\, dE \tag{19}$$

where $k_{cb,0}$ and $k_{ss,0}$ are energy-independent rate constants for electron transfer via the conduction band and via surface states, respectively.

Simulation results illustrating the effect of changing E_C while keeping other parameters constant are presented in Figure 8a. It is found that the plots consist of two distinct regions: at low I_0 the semilogarithmic plots are linear with slopes of $2.303 \times k_B T_{ss}/q$, and at high I_0 plots tend to a slope of $2.303 \times k_B T/q$ (i.e., 59 mV/decade at 298 K). Changing E_C simply changes the photovoltage at which the change in slope occurs. The same effect can also be achieved by altering the values of k_{cb} and k_{ss} (not shown).

Clearly the experimental data (Figure 6) cannot be well fitted using this approach without allowing the value of T_{ss} (which is the sole determinant of $dV_{OC}/d\log(I_0)$ at low I_0 in this model) to vary. The effect of varying T_{ss} for constant E_C is illustrated in Figure 8b. We find it is possible to approximately fit the experimental data using this simplified model if *both* T_{ss} and E_C are allowed to vary; however, the values of T_{ss} are required to vary between 410 and 300 K (corresponding to mean slopes which fall in the range 80−59 mV/decade) as $[Li^+]$ is increased. These values are significantly lower than the values of T_0 derived from the EIS experiments (671−1216 K), and the required trend in T_{ss} with $[Li^+]$ is *opposite* to the trend found for the T_0 values. We therefore conclude that this simpler model fails to adequately reproduce the $V_{OC}-I_0$ characteristics using reasonable estimates for T_{ss}. As such, use of the more complex Marcus−Gerischer model and the associated introduction of an additional fitting parameter, λ, appears to be justified in the present case.

Based upon these fitting and simulation results, it seems reasonable to assume that the variation in the $V_{OC}-I_0$ plots is caused by variation in the TiO_2 conduction band edge energy as a result of adsorption of Li^+ at the TiO_2−electrolyte interface. For values of E_{ox} (i.e., $E_{F,redox} + \lambda$) lower than E_C (as in the present case), transfer of conduction band electrons to electrolyte acceptor species can be considered to be in the so-called

"Marcus inverted region".[19] This results in sluggish electron transfer from the conduction band and leads to recombination occurring predominantly through band gap surface states, whose energies better match those of electron acceptors in solution. Upon shifting the band edge toward the electrolyte redox level, conduction band transfer becomes progressively more favorable as a result of better energetic matching between the conduction band edge and electron acceptor energy levels. The ratio of conduction band electrons to electrons occupying surface states is also increased at any given V_{OC} as the conduction band edge is lowered (for $T_{ss} > T$), further adding to the conduction band recombination flux. The combination of these factors leads to a gradual transition from surface-state-mediated recombination to conduction-band-mediated recombination as the band edge is lowered. Changes in the slopes of the $V_{OC}-I_0$ plots with varying $[Li^+]$ can be attributed to variation in the overlap between electron acceptor states in the electrolyte and the band gap surface state distribution. These concepts are illustrated in Figure 9.

Conclusions

Addition of Li^+ to the electrolyte of DSCs increases the electron injection efficiency across all wavelengths, with a particularly marked increase at longer wavelengths leading to an increase in photocurrent onset wavelength. Once $[Li^+] = 0.1$ M, the injection efficiency for short wavelengths saturates but continues to increase at long wavelengths until $[Li^+] = 1$ M, when a constant injection efficiency of close to unity is achieved for all wavelengths absorbed by the sensitizer. The changes in injection efficiency are attributed to an increased driving force for electron injection or better energetic matching of sensitizer excited states with acceptor states in the TiO_2, caused by a downward shift in the TiO_2 energy levels as a result of specific adsorption of Li^+ at the TiO_2−electrolye interface. Interestingly this conclusion implies that in order to improve the long-wavelength response of DSCs, the electron injection efficiency at long wavelengths needs to be optimized in tandem with more common strategies such as increasing light scattering or improving the red absorption of the sensitizing dye.

EIS experiments suggest that a high concentration (1 M) of Li^+ in the electrolyte increases the electron diffusion length; however, even in the absence of Li^+ the electron diffusion length is sufficiently long to render charge collection close to 100% efficient in these cells. Given the recent controversy about measurement of the electron diffusion length is DSCs, we do not wish to suggest that the diffusion lengths obtained here are correct in an absolute sense; however, we do note that our data is consistent with an electron diffusion length which is greater than the TiO_2 layer thickness.

Variation of Li^+ concentration in the electrolyte is also found to systematically alter the mean slopes on semilogarithmic $V_{OC}-I_0$ and $j_{dark}-V_{bias}$ plots. The curvature and mean slopes of the semilogarithmic $V_{OC}-I_0$ plots can be explained by assuming that recombination occurs through both the conduction band of the TiO_2 and an exponential distribution of surface states. The decreasing mean slopes and increase in linearity of the semilogarithmic $V_{OC}-I_0$ plots with increasing $[Li^+]$ is modeled well using the Marcus−Gerischer model of electron transfer and by allowing the energy of the TiO_2 conduction band with respect to the electrolyte redox level to vary, while keeping all other model parameters fixed. A simpler model, which neglects the effect of a distribution of electron acceptor species in the electrolyte, was found to be inadequate for fitting the $V_{OC}-I_0$ data without resorting to an unjustifiable variation in the energetic distribution of surface states as well as a shift in the conduction band edge.

Acknowledgment. This work was supported by NUS and Nanocore start-up grants (R-284-000-064-133/R-284-000-066-646) and FRC research grant (R-284-000-068-112). We acknowledge useful discussions with Yeru Liu.

Supporting Information Available: Current−voltage characteristics (AM 1.5, 0.96 Sun) of the DSCs used in this study, variation of the mean slopes of semilogarithmic R_t-V_{cell} and $R_{ct}-V_{cell}$ plots with $[Li^+]$, and absorbance spectra of dye-sensitized TiO_2 layers filled with electrolytes containing 0 to 1 M Li^+. This material is available free of charge via the Internet at http://pubs.acs.org.

References and Notes

(1) Oregan, B.; Gratzel, M. *Nature* **1991**, *353*, 737.
(2) Chiba, Y.; Islam, A.; Watanabe, Y.; Komiya, R.; Koide, N.; Han, L. Y. *Jpn. J. Appl. Phys., Part 2* **2006**, *45*, L638.
(3) Koops, S. E.; O'Regan, B. C.; Barnes, P. R. F.; Durrant, J. R. *J. Am. Chem. Soc.* **2009**, *131*, 4808.
(4) Haque, S. A.; Palomares, E.; Cho, B. M.; Green, A. N. M.; Hirata, N.; Klug, D. R.; Durrant, J. R. *J. Am. Chem. Soc.* **2005**, *127*, 3456.
(5) Heimer, T. A.; Heilweil, E. J.; Bignozzi, C. A.; Meyer, G. J. *J. Phys. Chem. A* **2000**, *104*, 4256.
(6) Barnes, P. R. F.; Anderson, A. Y.; Koops, S. E.; Durrant, J. R.; O'Regan, B. C. *J. Phys. Chem. C* **2009**, *113*, 1126.
(7) Moser, J. E.; Gratzel, M. *Chimia* **1998**, *52*, 160.
(8) Barnes, P. R. F.; Liu, L.; Li, X.; Anderson, A. Y.; Kisserwan, H.; Ghaddar, T. H.; Durrant, J. R.; O'Regan, B. C. *Nano Lett.* **2009**, *9*, 3532.
(9) Kopidakis, N.; Benkstein, K. D.; van de Lagemaat, J.; Frank, A. J. *J. Phys. Chem. B* **2003**, *107*, 11307.
(10) Bisquert, J.; Vikhrenko, V. S. *J. Phys. Chem. B* **2004**, *108*, 2313.
(11) Sodergren, S.; Hagfeldt, A.; Olsson, J.; Lindquist, S. E. *J. Phys. Chem.* **1994**, *98*, 5552.
(12) Halme, J.; Boschloo, G.; Hagfeldt, A.; Lund, P. *J. Phys. Chem. C* **2008**, *112*, 5623.
(13) Wang, H.; Peter, L. M. *J. Phys. Chem. C* **2009**, *113*, 18125.
(14) Bisquert, J.; Garcia-Belmonte, G.; Fabregat-Santiago, F.; Ferriols, N. S.; Bogdanoff, P.; Pereira, E. C. *J. Phys. Chem. B* **2000**, *104*, 2287.
(15) Bisquert, J. *J. Phys. Chem. B* **2002**, *106*, 325.
(16) Fabregat-Santiago, F.; Garcia-Belmonte, G.; Bisquert, J.; Zaban, A.; Salvador, P. *J. Phys. Chem. B* **2002**, *106*, 334.
(17) Wang, Q.; Ito, S.; Gratzel, M.; Fabregat-Santiago, F.; Mora-Sero, I.; Bisquert, J.; Bessho, T.; Imai, H. *J. Phys. Chem. B* **2006**, *110*, 25210.
(18) Peter, L. M. *J. Phys. Chem. C* **2007**, *111*, 6601.
(19) Bisquert, J.; Zaban, A.; Greenshtein, M.; Mora-Sero, I. *J. Am. Chem. Soc.* **2004**, *126*, 13550.
(20) Salvador, P.; Hidalgo, M. G.; Zaban, A.; Bisquert, J. *J. Phys. Chem. B* **2005**, *109*, 15915.
(21) Cameron, P. J.; Peter, L. M. *J. Phys. Chem. B* **2005**, *109*, 7392.
(22) Cameron, P. J.; Peter, L. M.; Hore, S. *J. Phys. Chem. B* **2005**, *109*, 930.
(23) Jennings, J. R.; Ghicov, A.; Peter, L. M.; Schmuki, P.; Walker, A. B. *J. Am. Chem. Soc.* **2008**, *130*, 13364.
(24) Mora-Sero, I.; Bisquert, J. *Nano Lett.* **2003**, *3*, 945.
(25) Bisquert, J.; Fabregat-Santiago, F.; Mora-Seroİ, I. n.; Garcia-Belmonte, G.; Gimeİnez, S. *J. Phys. Chem. C* **2009**, *113*, 17278.
(26) Bisquert, J.; Zaban, A.; Salvador, P. *J. Phys. Chem. B* **2002**, *106*, 8774.
(27) Duggleby, R. G. *Anal. Biochem.* **1990**, *189*, 84.

JP9104129